EPR investigation of N@C_70 in polycrystalline C_70 and single wall carbon nanotubes

Klaus-Peter Dinse, Björn Corzilius, Peter Jakes, Norbert Weiden, Suman Agarwal

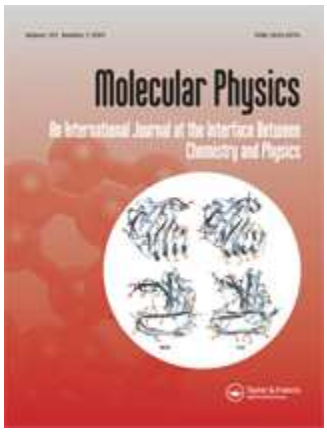

EPR investigation of N@C$_{70}$ in polycrystalline C$_{70}$ and single wall carbon nanotubes

Journal:	*Molecular Physics*
Manuscript ID:	TMPH-2007-0182.R1
Manuscript Type:	Full Paper
Date Submitted by the Author:	15-Aug-2007
Complete List of Authors:	Dinse, Klaus-Peter; TU Darmstadt, Chemistry Corzilius, Björn; TU Darmstadt, Chemistry Jakes, Peter; TU Darmstadt, Chemistry Weiden, Norbert; TU Darmstadt, Chemistry Agarwal, Suman; TU Darmstadt, Chemistry
Keywords:	Single wall carbon nanotubes, N@C$_{70}$, EPR
Note: The following files were submitted by the author for peer review, but cannot be converted to PDF. You must view these files (e.g. movies) online.	
NC70_7.tex	

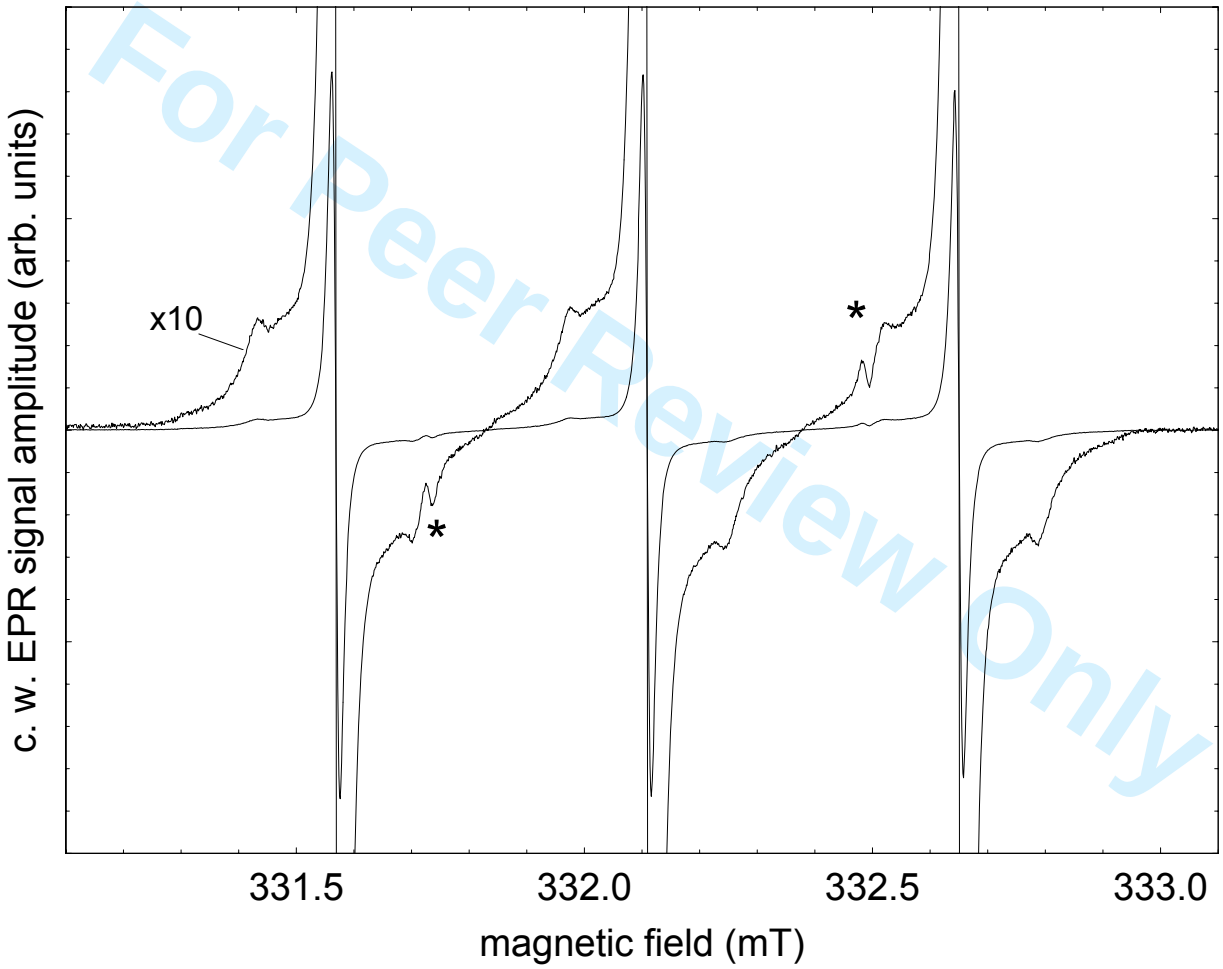

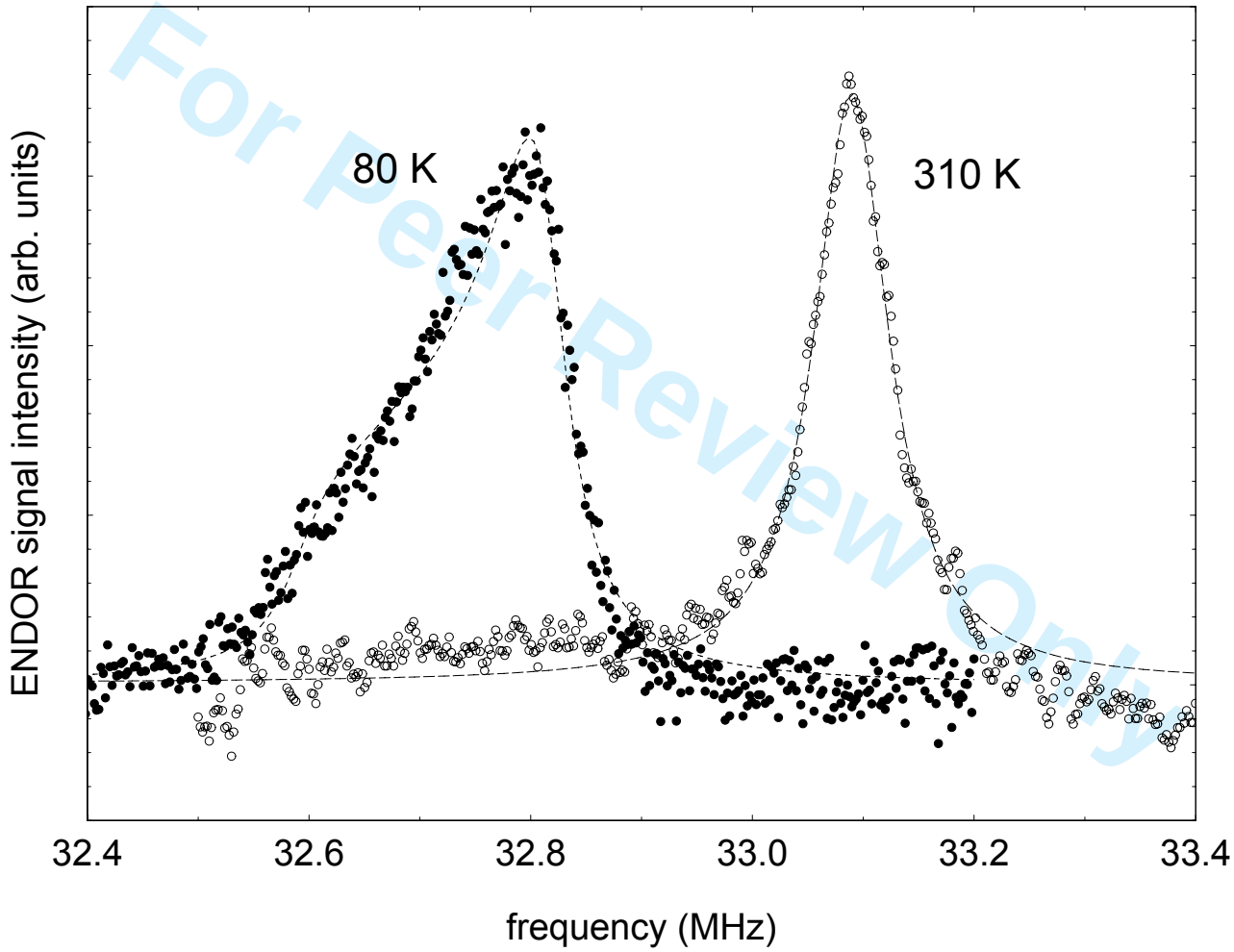

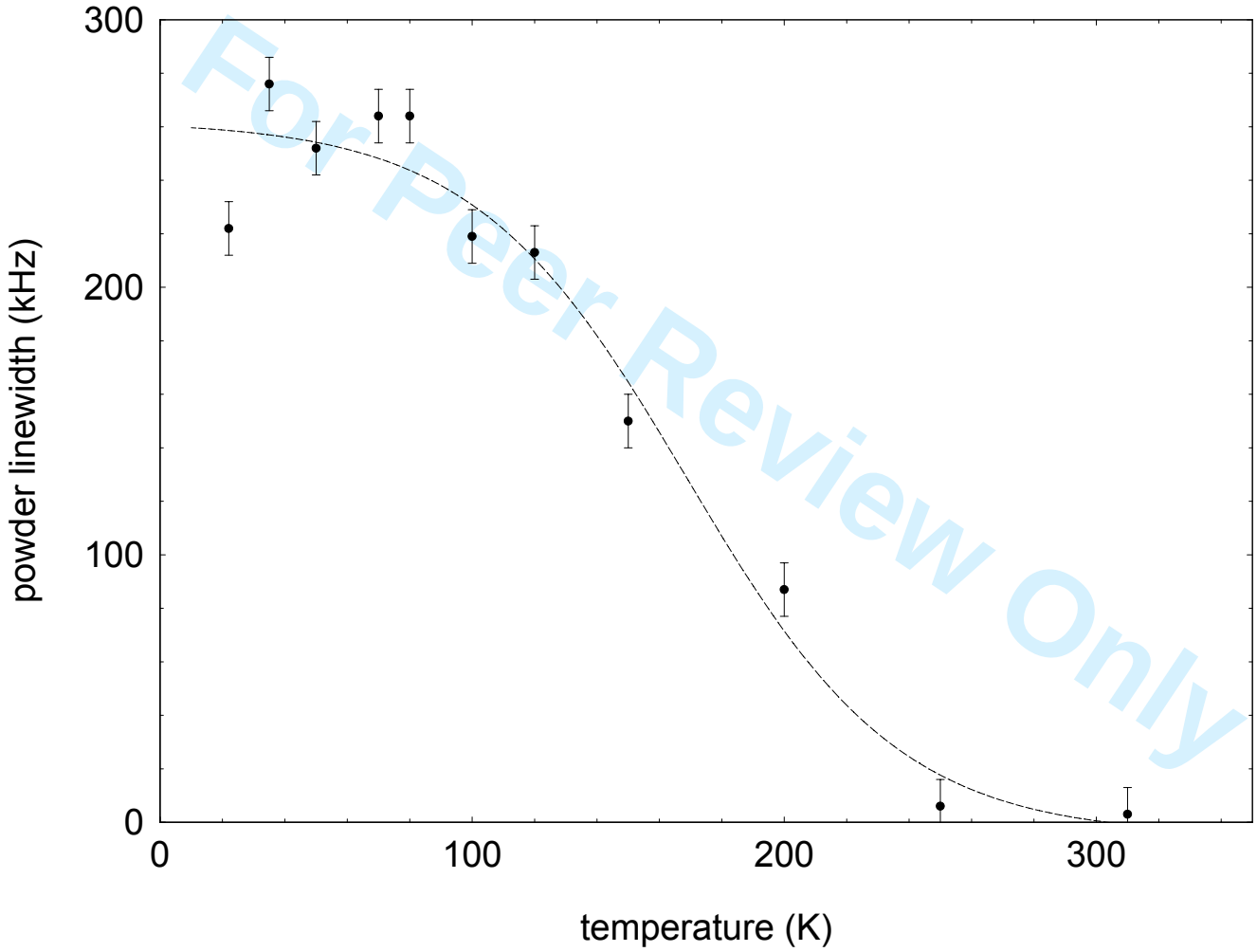

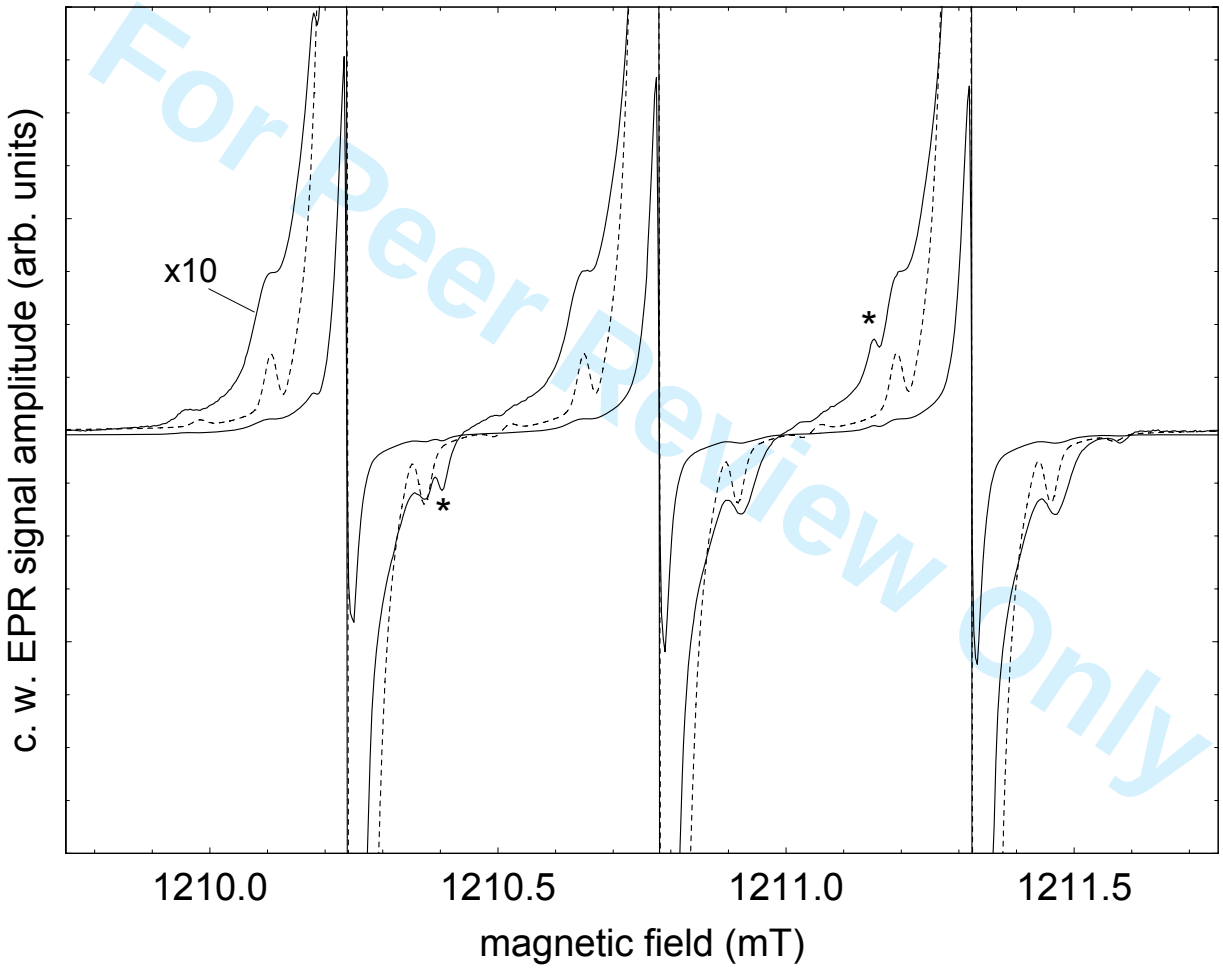

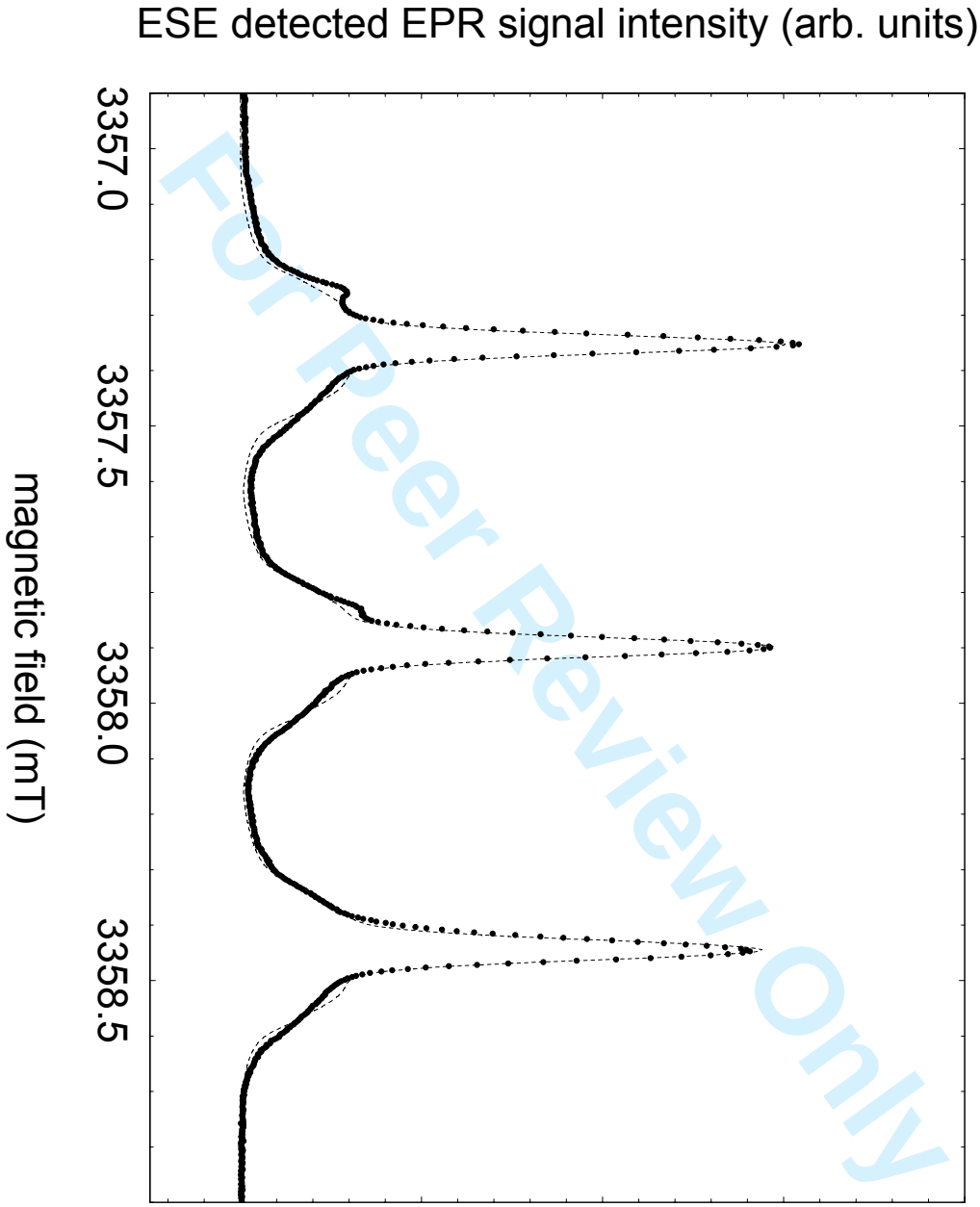

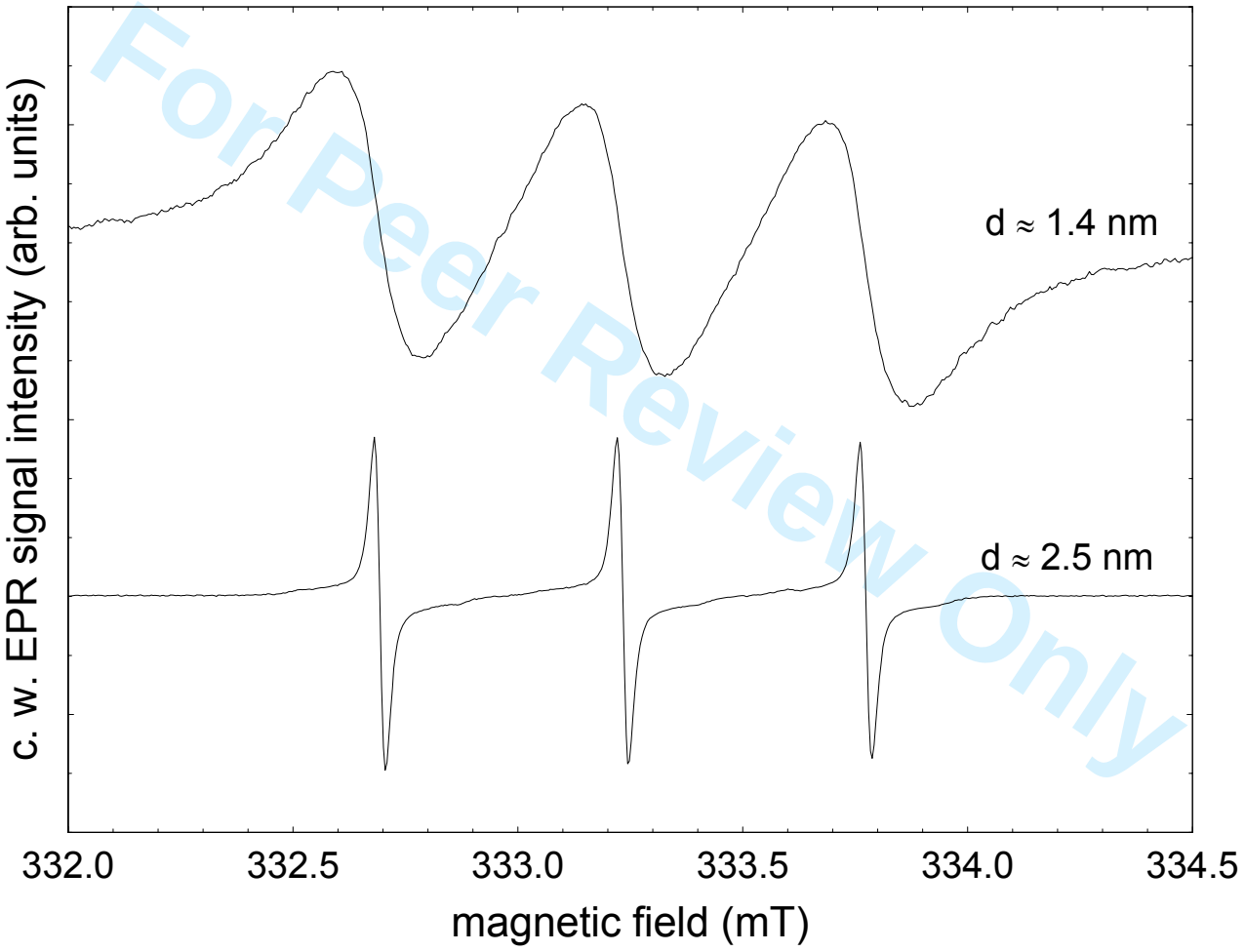

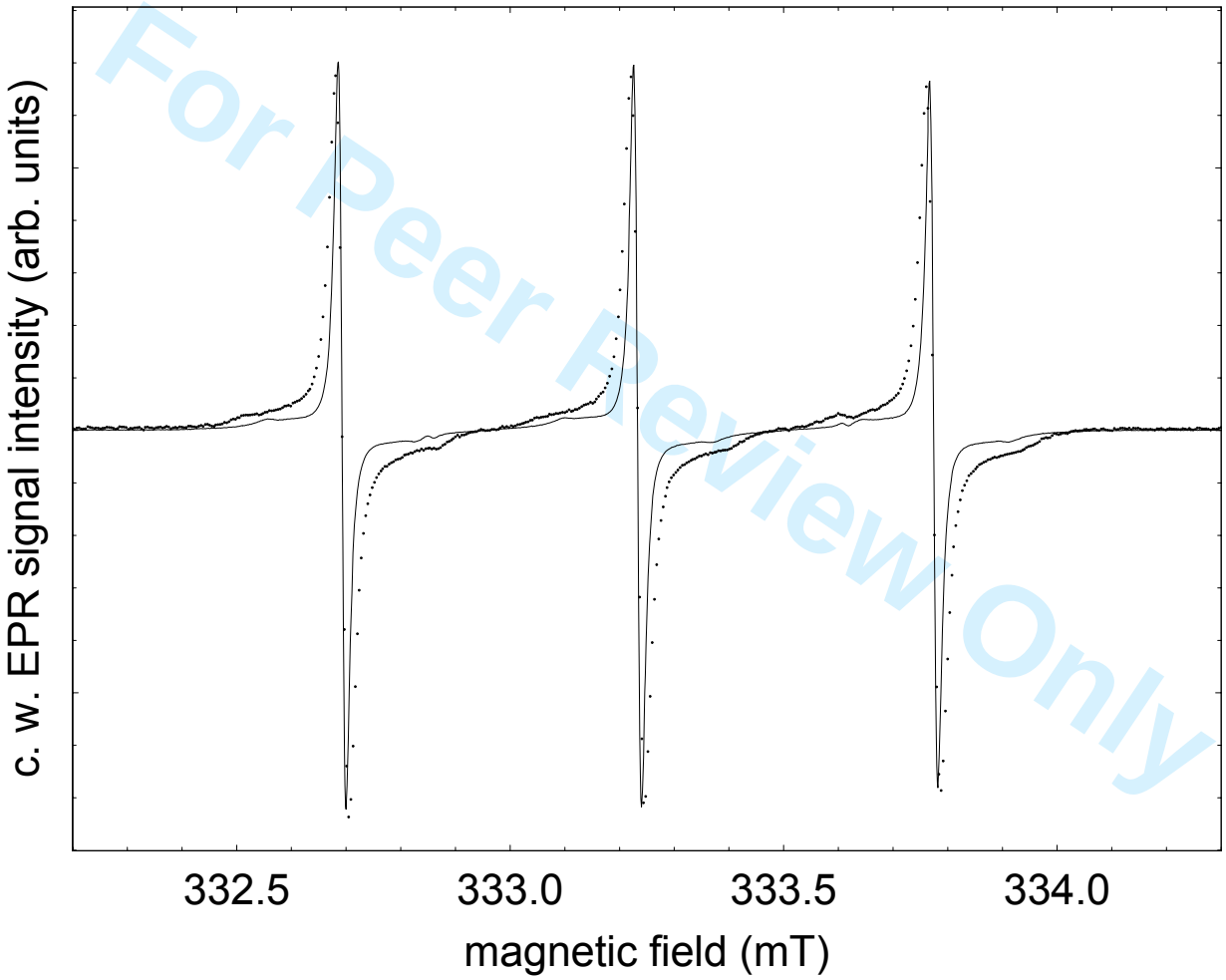

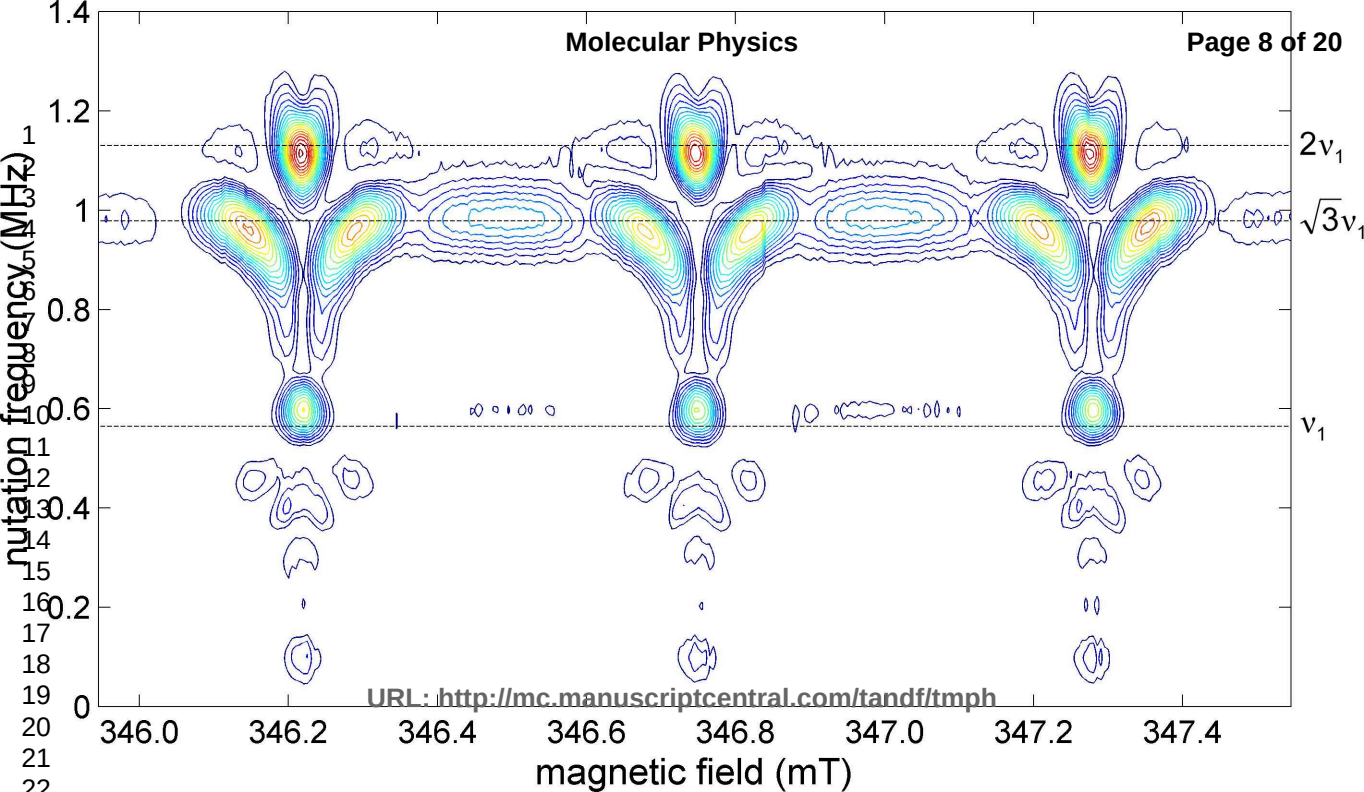

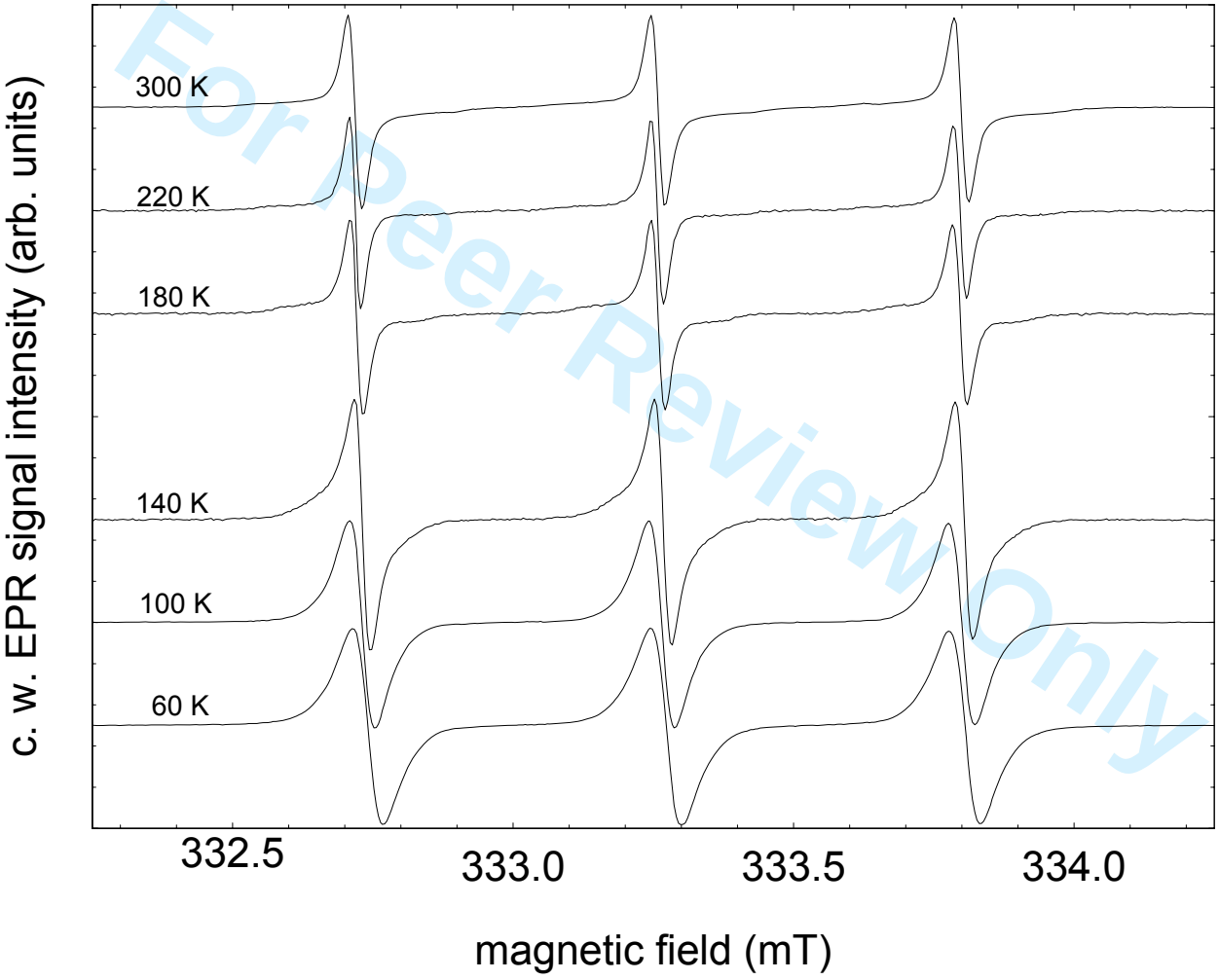

Molecular Physics, Vol. 00, No. 00, DD Month 200x, 1–11

EPR investigation of N@C_{70} in polycrystalline C_{70} and single wall carbon nanotubes

B. CORZILIUS†, P. JAKES†, N. WEIDEN†, S. AGARWAL†‡, and K.-P. DINSE*†

† Physical Chemistry III, Technical University Darmstadt, Petersenstrasse 20, D-64287 Darmstadt, Germany

‡ Department of Chemistry, Indian Institute of Technology, Hauzkhas, New Delhi 110016, India

(*Received 00 Month 200x; in final form 00 Month 200x*)

Using multi frequency electron paramagnetic resonance (EPR) it was possible to determine the inherent fine structure (FS) interaction of nitrogen encapsulated in a C_{70} cage. Confinement of N@C_{70} in single wall carbon nanotubes (SWNT) of rather wide diameter does not significantly influence this value. The transition between isotropic molecular tumbling and immobilisation was found to occur at about 170 K in both matrices, indicating that the hindrance potential is quite small in both cases.

Keywords: (Single wall carbon nanotubes; N@C_{70}; EPR)

1 Introduction

Since the discovery of fullerenes encapsulated in carbon nanotubes ('peapods') [1], many metallo-endohedral fullerene (MEF)-based peapods have been synthesised and characterised by X-ray techniques [2]. Not only clear proof of encapsulation was provided but furthermore information about metal reorientation and escape from the fullerene cage has been documented [3–5]. No clear electron paramagnetic resonance (EPR) signature of such compounds has been obtained, probably because of reductive or oxidative charge transfer between MEF and nanotube, giving rise to spin delocalisation. In contrast, it was shown by EPR that endohedral N@C_{60} and N@C_{70} are much much less influenced by incorporation into single wall carbon nanotubes (SWNT) [6, 7], because the repulsive potential between fullerene cage and nitrogen atom prevents any significant charge and spin transfer to the cage [8], thus preventing spin delocalisation. Under these conditions, the quartet electron spin of the encapsulated nitrogen atom in its electronic ground state can be used to search for dynamic reorientation on the time scale of EPR. In particular, the inherent FS interaction generated by the ellipsoidal C_{70} cage can be utilised to search for a transition between isotropic tumbling and orientational disorder.

Because of spin relaxation times in the microsecond range even at room temperature [9], N@C_{60} and N@C_{70} based peapods not only can be investigated by standard continuous wave (c. w.) EPR but also by pulsed EPR techniques, providing additional insight into details of the fluctuating interactions.

*Corresponding author. Email: dinse@chemie.tu-darmstadt.de

Molecular Physics
ISSN 00268976 print/ISSN 13623028 online © 200x Taylor & Francis
http://www.tandf.co.uk/journals
DOI: 10.1080/0026897YYxxxxxxxx

2 Experiment

Endohedral fullerenes $N@C_{70}$ were prepared using the ion implantation technique described elsewhere [10]. Enrichment of the endohedral fullerenes was performed using high performance liquid chromatography [11], resulting in $N@C_{70}$ material with concentrations of up to 4 %, respectively. Polycrystalline C_{70} doped with $N@C_{70}$ was obtained by crystallisation out of a CS_2 solution.

SWNT of 1.4 nm mean diameter produced by arc discharge method were purchased from Carbon Solutions Inc. (USA). Due to the high amount of remaining Ni/Y catalyst, purification consisting of repeated dry oxidation and acid treatment steps, as was reported earlier [7, 12], was mandatory. SWNT with an average diameter of 2.5 nm were produced by ethylene chemical vapor deposition (CVD) as described elsewhere [13]. The main advantage of this 'super-growth' method is the easy way to obtain catalyst free SWNT samples. When peeling off the SWNT forest from the substrate plate, the iron catalyst remains on the substrate. So one can obtain pure (more than 99.9 % carbon) SWNT without the need of further purification.

$N@C_{70}$ peapods were prepared following the procedure by Yudasaka et al. [14]. Typically 5 mg of the endohedral fullerene were ultrasonically dispersed in 50 mL ethanol (abs.). Instead of using the as grown tubes, the material has been heated in air to 500 °C for 30 min prior to fullerene incorporation to improve the filling efficiency. 5 mg of pretreated SWNT material were added and the flask was sealed. After 24 h the supernatant ethanol was removed. The powder was dried in vacuum and suspended in toluene so that the outside fullerenes were removed by dissolution. The suspension was filtered, the solid washed thoroughly with toluene and dried in air.

EPR measurements were performed using Bruker ESP 300E X-band and Q-band c. w. spectrometers operating at microwave (mw) frequencies of 9.4 GHz and 34 GHz, as well as using an ElexSys E680 system for c. w. and pulsed experiments at 9.7 GHz and 94 GHz. For the c. w. X-band spectrometer rectangular cavities (Bruker ER 4102ST or ER 4104OR, TE_{102} mode, respectively) served as resonator, temperature dependent measurements were done with a liquid helium flux cryostat (Oxford ESR 900). Q-band experiments were performed with a cylindrical resonator ER 5106QT (TE_{011} mode) immersed in a helium flow cryostat (Oxford CF935STD). In the ElexSys system the sample tubes could be inserted in a cylindrical cavity (Bruker ER 4118X-MD5, TE_{011} mode) for X-band experiments and in a cylindrical TE_{011} cavity of a standard Bruker probehead for W-band experiments. W-band electron nuclear double resonance (ENDOR) experiments were performed using a home-built resonator [15]. Temperature control was achieved with a helium flow cryostat (Oxford CF935STD).

3 Results and discussion

3.1 *Continuous wave EPR of $N@C_{70}$ in polycrystalline C_{70}*

The exceptional rotational mobility of C_{60} in single crystals and polycrystalline material at room temperature has been detected with various techniques. Isotropic rotational diffusion was observed above 255 K, defining a phase transition to a low temperature phase characterised by a low site symmetry and restricted rotation. This reduction of symmetry at the centre of the fullerene cage was detected by the resulting FS interaction sensed by the quartet state of encapsulated nitrogen atoms [9]. Early attempts to identify the anticipated analogous behaviour of C_{70}

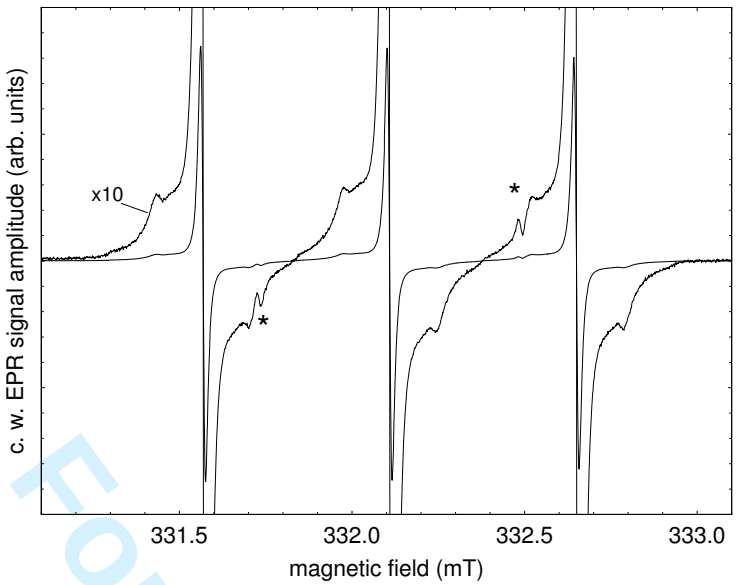

Figure 1. X-band c. w. EPR spectrum of N@C_{70} in polycrystalline C_{70} taken at room temperature. Signals originating from ^{15}N are indicated by an asterisk. To facilitate identification of additional structures, the signal is also shown after magnification by a factor 10.

by EPR were less successful, probably because of inferior sample quality indicated by inhomogeneous line broadening. As result, the transformation of the powder EPR spectrum expected for an immobilised C_{70} cage into a solution-like spectrum at elevated temperatures could not be observed with certainty.

Using material of higher relative N@C_{70} concentration and improving the C_{70} purity, we now recorded EPR spectra with improved spectral resolution. At room temperature the expected narrow lines were observed, indicating fast isotropic reorientation (see Fig. 1). Displaying the same spectrum by changing the vertical scale, signals of ^{15}N@C_{70} occurring in natural abundance as well as weak shoulders are also displayed. It is tempting to interpret these shoulders in Fig. 1 as 'van Hove singularities' of the perpendicular orientation, although this would not be compatible with the assumption of fast isotropic motional averaging predicted for $T = 300$ K. Clear evidence for such a transition from fast uniaxial rotation to isotropic motion at a much lower temperature of about 180 K in a C_{70} matrix was obtained from an analysis of ^{13}C hyperfine interaction (hfi) in muon spin resonance data of $\mu C_{70}^{\bullet}$ radicals [16]. It was also noted that fast rotation about the long molecular axis persists down to 70 K. Because this information was obtained when investigating the muon adduct of C_{70}, it is reasonable to assume that the unmodified cage might exhibit an even lower transition temperature, thus prohibiting the observation of a rigid limit powder pattern for our sample.

In order to verify the predicted phase transition for the unmodified cage, we measured the nitrogen hfi using high resolution pulsed ENDOR techniques. The principal axes of the nitrogen dipolar and quadrupolar hyperfine tensors are determined by the orientation of the long cage axis. The anticipated transition from anisotropic to isotropic hfi can be detected by searching for a collapse of the characteristic powder ENDOR line shape. As was shown previously [15], the rigid limit anisotropic part of the dipolar and quadrupolar nitrogen hfi is only of the order of 200 kHz, being a small perturbation to the isotropic part of about 15 MHz. Under these conditions, line narrowing as function of temperature can be analyzed and the temperature of rotational melting can be easily determined. By this method a direct measure of the dynamics of the long cage axis of an unmodified cage can be obtained.

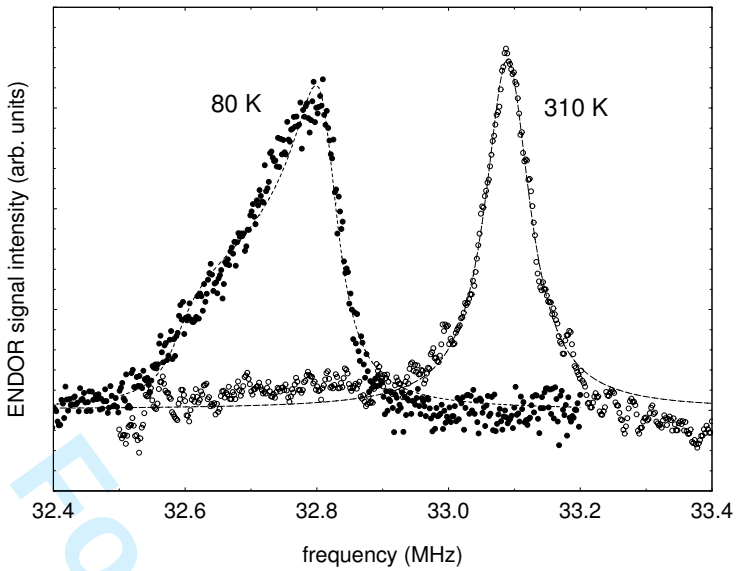

Figure 2. W-band ENDOR spectra of N@C_{70} in polycrystalline C_{70}. The nitrogen ENDOR transition shown occurs within the $m_S = -3/2$ manifold, when exciting the low field ($m_I = +1$) EPR transition.

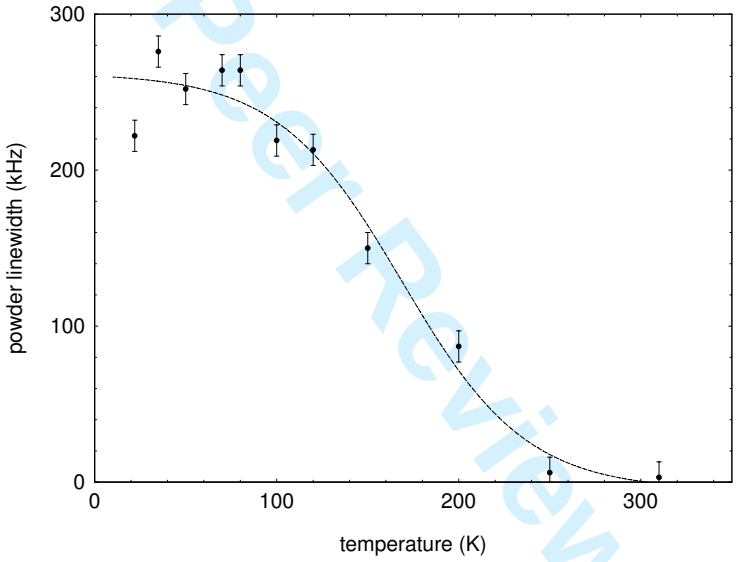

Figure 3. Temperature dependence of the nitrogen hfi anisotropy in polycrystalline C_{70}.

In Fig. 2, one of the four ^{14}N ENDOR transitions is shown, measured by pulsed ENDOR in W-band (94 GHz) at 80 K and 310 K. The microwave pulse sequence used was $0.4 - 110 - 0.2 - 3 - 0.4$ μs (indicating pulse lengths and delay times, respectively). The rf pulse length was 100 μs in order to optimize spectral resolution, the power used was approximately 500 W. The chosen temperatures are well below and above the anticipated phase transition. The line observed at low temperature can be fitted by assuming hfi of axial symmetry. In the high temperature limit, the ENDOR line is of Lorentzian shape. The observed anisotropy of the hfi gradually decreases, as is depicted in Fig. 3. Its temperature dependence can be described with an approximate transition temperature of 168 K, similar to the value determined previously by μSR. It is therefore safe to conclude that 'orientational melting' occurs at this temperature and that at room temperature no zero field splitting (ZFS) caused powder pattern should be observable.

Q-band spectra of the same sample were also measured to check for a possible field dependence of the additional lines. The room temperature spectrum is dis-

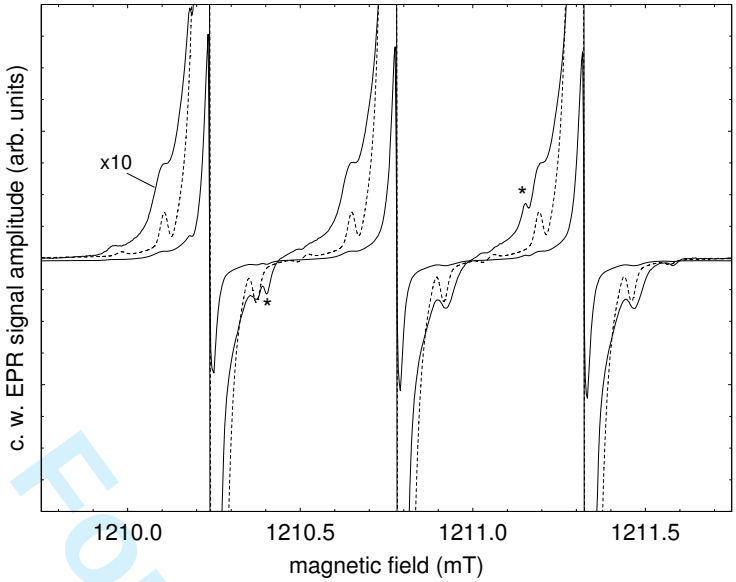

Figure 4. Q-band c. w. EPR spectrum of N@C_{70} in polycrystalline C_{70} taken at room temperature. Signals originating from ^{15}N are indicated by an asterisk. To facilitate identification of additional structures, the signal is also shown after magnification by a factor 10. As dotted curve a spectral simulation is shown assuming a relative intensity of 1:15 for the unspecified N@C_{70} adduct.

played in Fig. 4, clearly showing the same pattern as observed at 9.4 GHz. By changing the Larmor frequency it can be excluded that the additional lines are caused by forbidden transition, which could originate from distant ^{13}C nuclei in natural abundance. (The frequency separation of 3.6 MHz of the 'prominent' lines would only match well with the free nuclear Zeeman frequency of ^{13}C spins in X-band (3.55 MHz at 332 mT).)

Because of the observed independence of the powder pattern and its constant relative intensity ratio when using two different electronic Larmor frequencies, we are therefore led to assign the observed shoulders as arising from ZFS interaction. The very weak intensity of the 'shoulders', however, is not compatible with any simulation of a ZFS powder pattern, but rather indicates that it is caused by an additional compound. Because of the well founded prediction that C_{70} cages would quickly reorient at room temperature, we therefore suggest that the strong central line originates from N@C_{70} under isotropic tumbling conditions and that the weak shoulders are caused by an additional compound, probably a N@C_{70} adduct. The presence of any bulky side chain would prevent fast reorientation even at 300 K. This assignment is supported by the observation that the principal component of the ZFS constant $|D| = 3.6(1)$ MHz, obtained by simulation of X- and Q-band spectra, is not in agreement with an estimate of -2.6(3) MHz, deduced from the analysis of EPR spectra obtained in the nematic phase of a liquid crystal [17].

From Fig. 3 it is obvious that the transition from uniaxial rotation to free isotropic tumbling is extended over a wide temperature range. We therefore expected that an analysis of the EPR spectrum taken at the rather high Larmor frequency of 94 GHz would be better suited to show the ZFS caused powder pattern at elevated temperatures, because the correlation time describing the reorientation of the long axis of the cage would not be in the sub picosecond range even close to room temperature. Apart from shifting the temperature range in which rigid limit conditions are fulfilled to higher temperatures, an additional advantage in the use of W-band EPR is given by the fact that the effect of an anisotropic Zeeman interaction is much larger, thus leading to a characteristic asymmetry of the EPR spectrum. This feature would allow unambiguous identification of all parts of the

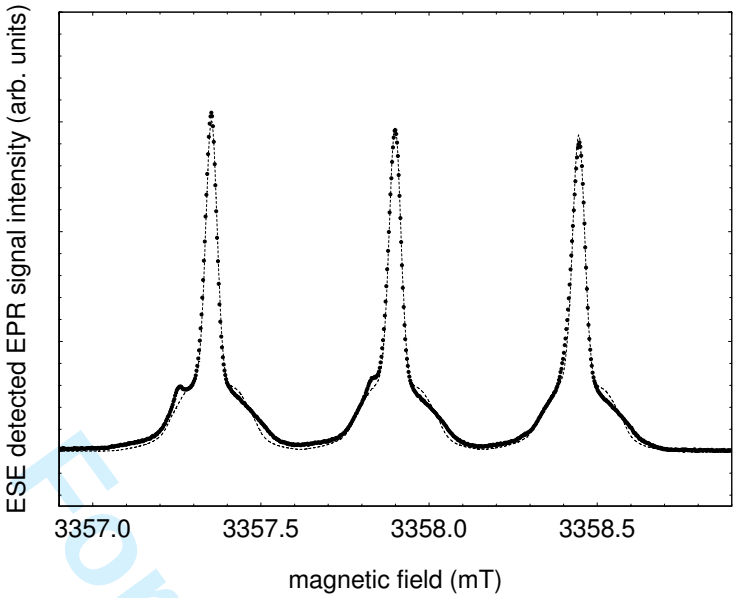

Figure 5. Experimental and simulated (dashed line) echo detected W-band EPR spectrum of N@C_{70} in polycrystalline C_{70} ($T = 300$ K). The pulse sequence used was $0.18 - 3 - 0.2$ μs.

spin Hamiltonian.

In the 94 GHz spectrum, which was detected by recording the 2-pulse Hahn echo under field sweep conditions, the intensity of the powder pattern relative to the central transition is now much larger. This observation indicates that the rotational correlation time of the main component, i. e., of unmodified N@C_{70} is still not short compared to the reciprocal Larmor frequency. As shown in Fig. 5, the expected asymmetry of the powder pattern, resulting from g matrix anisotropy is clearly visible. We confirmed by simulation that the asymmetry of the powder pattern is caused by a small g matrix anisotropy ($\Delta g = 10^{-5}$). The small intensity difference of hyperfine components originates from the anisotropy of the nitrogen hfi ($\Delta A = 150$ kHz) in combination with the g anisotropy. (The numerical value for $A(^{14}\mathrm{N})$ is taken from previous ENDOR results [15].) It was also necessary to allow for a certain distribution of ZFS parameters in order to match the ratio of intensities of the narrow central transition to the 'powder' pattern. Simulation parameters are listed in Table 1. It is noteworthy that D of the major compound is significantly smaller than the value determined for the adduct. The negative sign of D listed in Table 1 was previously determined by evaluating second order effects in highly resolved EPR spectra of N@C_{70} in the nematic phase of a liquid crystal [17]. The value determined for D by spectral analysis is less by a factor 2 than the value estimated from a recent analysis of the temperature dependence of relaxation rates [18]. Because of the close agreement with the value determined for N@C_{70} in SWNT (see below), we believe that the direct determination of D by spectral analysis yields more reliable results.

The relative order of g matrix elements is determined using Eq. (1), by which the peak intensity reduction of the high field hyperfine component (hfc) is related to a linear m_I effect for the broadening of the central component of each hfc. For this analysis ENDOR determined values for $A(^{14}\mathrm{N})$ (including sign) have been used.

$$\mathrm{sign}(g_{\parallel} - g_{\perp}) = -\mathrm{sign}(A_{\parallel} - A_{\perp}) \qquad (1)$$

Table 1. Spin Hamiltonian parameters used for spectral simulation of the 94 GHz spectrum. The data of the major component (N@C_{70}) are listed in the first line of the table. The spectrum of the minor component, which is simulated with entries of the second line is multiplied by a factor 1/15.

$A_\parallel$ (MHz)	$A_\perp$ (MHz)	$g_\parallel$	$g_\perp$	D^a (MHz)	E^a (MHz)	line width$_{(FWHM)}$(mT)
15.18	15.33	2.00001	2.00000	-2.6(9)	0.0(2)	0.04
15.18	15.33	2.00001	2.00000	-3.6(1)	0.0	0.02

[a]The half width of the Gaussian distribution of D and E values used in the simulation is indicated in parentheses.

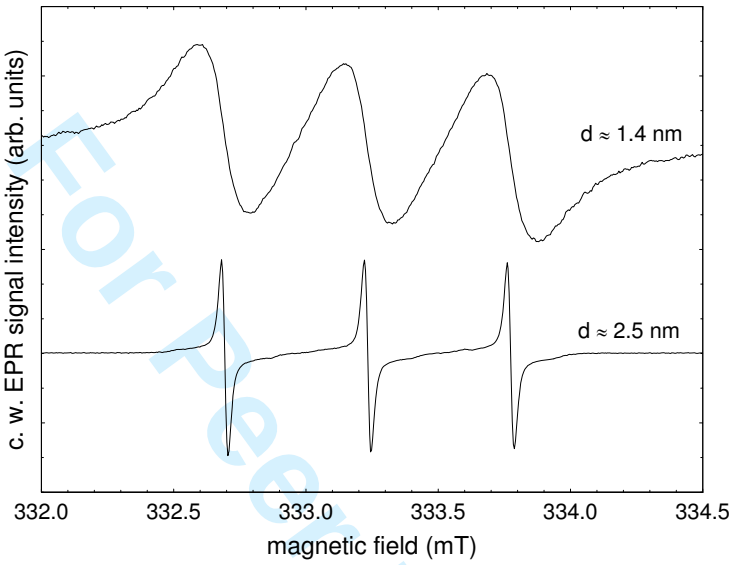

Figure 6. X-band EPR spectra of N@C_{70} in SWNT of different diameter ($T = 300$ K).

3.2 *EPR of N@C_{70} derived peapods*

As we reported in a previous study, a significant reduction of the inhomogeneous line width of N@C_{60}-derived peapods is observed, when increasing the diameter of SWNT from approximately 1.4 nm to 2.5 nm [19]. A similar effect was expected to occur also for N@C_{70}. In Fig. 6, X-band spectra of N@C_{70}-derived peapods using tubes of different diameter are compared. The anticipated reduction of the line width is indeed observed for N@C_{70}. Whereas line broadening prevented observation of substructures when embedded in the 'narrow' tubes, weak additional structures can now be recognised when using wider diameter tubes for confinement. For a study of the hindered rotation of N@C_{70} in SWNT the use of the CVD grown material therefore is mandatory.

In Fig. 7, X-band EPR spectra are compared for N@C_{70} embedded in polycrystalline C_{70} and in SWNT of approximately 2.5 nm diameter. Apart from an increase in line width, the general features of the spectrum seem to be preserved, i. e., broad shoulders are present, extending by approximately 0.2 mT to both sides of the principal nitrogen hyperfine components. No change of ^{14}N hfi can be observed. Assuming that the presence of an additional compound is responsible in both cases, we can conclude that fast isotropic rotational tumbling occurs at room temperature in SWNT of approximately 2.5 nm diameter as well. Considering that the 'free' inner diameter of nominally 2.5 nm tubes amounts to about 2.2 nm, this is not really surprising.

When cooling the N@C_{70}@SWNT sample, a qualitative change of its EPR spectrum is observed at about 150 K (see Fig. 8). At this temperature, the width of the central component increases markedly from 0.02 to 0.05 mT. It is noteworthy

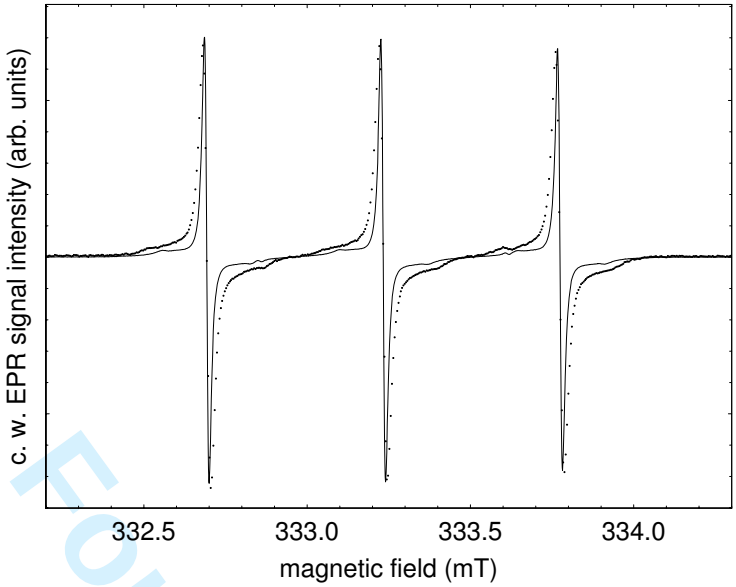

Figure 7. X-band EPR spectra of N@C_{70} in SWNT (dotted) and polycrystalline C_{70} (solid line) ($T = 300$ K).

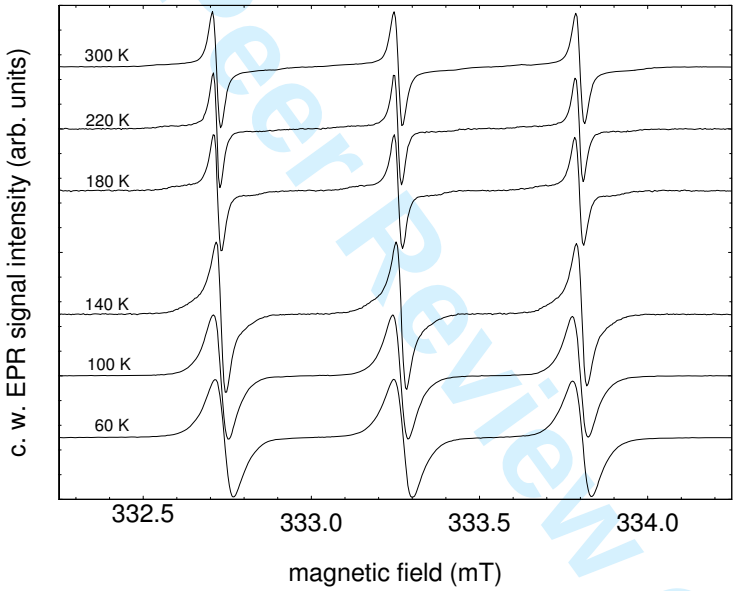

Figure 8. Temperature dependence of X-band EPR spectra of N@C_{70} in SWNT

that 150 K is very close to the rotational melting temperature, measured in the C_{70} matrix. We therefore assume that this fully reversible change also is related to orientational disorder of the long axis of the cage.

To confirm this conclusion, the detection and analysis of ZFS features expected at lower temperatures after immobilisation is required. Because no information about the ZFS interaction can be deduced from the low temperature c. w. EPR spectra, we used pulsed EPR techniques to search for differences in nutation frequencies, characteristic for a high spin system. Because of differences in magnetic transition moments between spin levels of the quartet spin system of N@C_{70}, the transitions between the $m_S = -1/2$ and $m_S = +1/2$ states can be separated from the transitions between the $m_S = -3/2$ and $m_S = -1/2$ and $m_S = +1/2$ and $m_S = +3/2$ states. In a spin nutation experiment, mw pulses of different lengths are applied in order to obtain different rotation angles of the macroscopic mag-

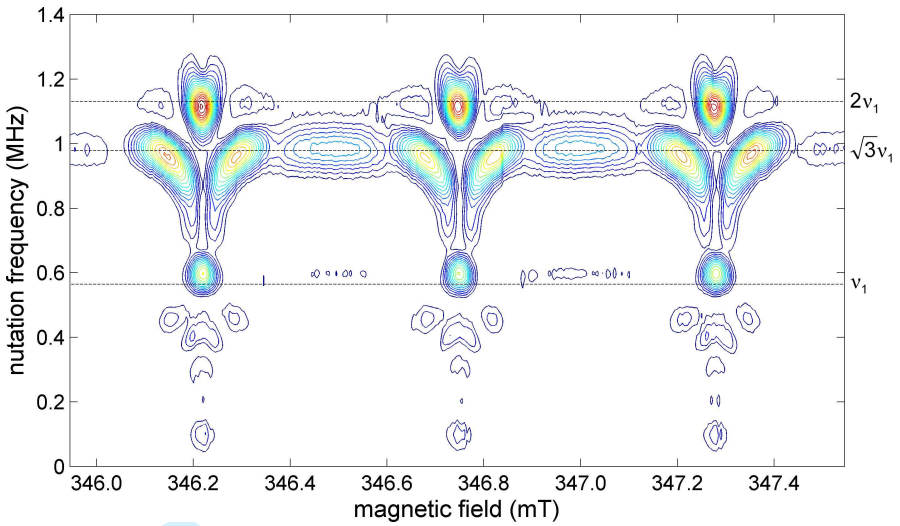

Figure 9. Absolute value FT of the phase inverted FID detected nutation experiment of N@C_{70} in SWNT. The relative nutation frequencies according to Table 2 are marked by dashed horizontal lines.

Table 2. Overview of the possible nutation frequencies in a $S = 3/2$ spin system.

Transition	$\nu_1 < \|D\|$	$\nu_1 > \|D\|$
$m_S = -3/2 \rightarrow -1/2$	$\sqrt{3}\nu_1$	ν_1
$m_S = -1/2 \rightarrow +1/2$	$2\nu_1$	ν_1
$m_S = +1/2 \rightarrow +3/2$	$\sqrt{3}\nu_1$	ν_1

netisation [20]. This results in an oscillation of the detection signal with respect to the pulse length. The most simple nutation experiment uses a standard FID detection sequence, with a subsequent elongation of the $\pi/2$ pulse length up to a few μs. Because of the increasing pulse length, the excitation bandwidth is decreasing during the experiment, which can lead to the formation of artifacts. Furthermore the effective time, in which spin relaxation can occur also varies. To avoid this, one long mw pulse of constant length $t_2 = 8$ μs is applied instead. Within this pulse the mw phase is shifted by 180° at time t_1, ranging from $t_1 = 0$ to $t_1 = t_2$ in steps of 64 ns. The field-dependent absolute value Fourier-transformed FID oscillations observed at 10 K are shown in Fig. 9.

For a $S = 1/2$ spin system, the Rabi frequency ν_1 determined by a mw field with amplitude B_{mw} is defined by

$$\nu_1 = \gamma_e B_{mw} \tag{2}$$

In practice, one has to distinguish between two cases: if ν_1 is smaller than the effective FS interaction of the spin system, spin packets forming the powder pattern can be excited selectively. As result, spins are nutating with ν_1 multiplied by the transition moment, being 2 for the $m_S = -1/2 \rightarrow +1/2$ transition and $\sqrt{3}$ for the $m_S = -3/2 \rightarrow -1/2$ and $m_S = +1/2 \rightarrow +3/2$ transitions, respectively. If the Rabi frequency is larger than the effective FS interaction, however, the complete ensemble is affected and the system behaves as a $S = 1/2$ system, i. e., rotating with ν_1 [21]. Possible nutation frequencies are compiled in Table 2.

All three predicted frequencies can be found in the spectrum in Fig. 9. Whereas signals at $2\nu_1$ and $\sqrt{3}\nu_1$ are expected for an inhomogeneously broadened powder spectrum of a $S = 3/2$ spin system, the occurrence of a signal at ν_1 is at first glance surprising. The signal found at $2\nu_1$ can be attributed to orientation independent $m_S = |1/2|$ transitions, defining the centre of the three hyperfine-split peaks with

a rather narrow width in the field-domain. At $\sqrt{3}\nu_1$, the maximum intensity is separated by approx. 0.15 mT, centred around the $m_S = |1/2|$ signal. This structure is caused by the FS splitting and it allows to extract an estimate for D from the 2-dimensional spectrum. Assuming that the peak positions originate from molecules in 'perpendicular' orientation because of maximised abundance, we obtain $D \cong 2.0(2)$ MHz. This value is close to the value determined for N@C_{70} in C_{70}, thus proving that the 'sensor' molecule is not significantly deformed by inclusion in the nanotube.

Because of the orientation dependence of the FS interaction, the effective splitting in a powder sample 'seen' by a molecule ranges from $-2D$ to $+D$ and $-D$ to $+2D$, respectively. As result, there are certain orientations, for which a very small or even vanishing effective FS splitting occurs, resulting in a switch over from the regime with $\nu_1 < |D|$ to the limit where $\nu_1 > |D|$ applies. This can be seen in Fig. 9, by observing that a signal located initially at $\sqrt{3}\nu_1$ rapidly is converted to a peak at the basic Rabi frequency ν_1, when approaching the resonance field of the $m_S = -1/2 \rightarrow +1/2$ transition. At these field values, the effective ZFS vanishes.

4 Conclusion

Using multi-frequency EPR as well as pulsed EPR techniques it was possible to investigate rotational melting of N@C_{70} embedded in polycrystalline C_{70} as well as in SWNT. In the former matrix, this transition should be marked by a conversion of the characteristic powder pattern of a $S = 3/2$ spin system into an 'isotropic' spectrum with narrow EPR lines. The small deviation from spherical symmetry of the C_{70} cage results in a small value for the principal component of the (axial) FS tensor. Because of its small size ($D = -2.6(3)$ MHz), no clear spectral features developed even for the C_{70} matrix with its well characterized crystal field. The analysis was further impeded by the presence of an N@C_{70} adduct with relative concentration of about 7 %, exhibiting a slightly larger FS interaction. Verification of the anticipated transition into a freely rotating state was finally obtained by using pulsed ENDOR techniques, by which the collapse of the anisotropic nitrogen hfi was detected instead.

Because of line broadening when using SWNT for confinement, the identification of FS caused spectral features was not possible using c. w. EPR. A final verification of the anticipated structure could be reached, however, by using the differences in magnetic transition moments for discrimination.

It was surprising that no significant difference with respect to long axis alignment in both 'matrices' could be detected. We therefore conclude that the nearly spherical N@C_{70} is probably localised at the inner wall of the nanotube and experiences fast thermally activated reorientation at this site. Future experiments are planned to investigate spin relaxation properties close to the transition temperature.

5 Acknowledgement

We thank K. Hata for the gracious supply of CVD 'super-growth' SWNT samples. Financial support by the 'Deutsche Forschungsgemeinschaft' (grant Di182/23) is gratefully acknowledged.

References

[1] B.M. Smith, M. Monthioux, D.E. Luzzi. *Nature,* **396**, 323 (1998).

[2] K. Hirahara, K. Suenaga, S. Bandow, H. Kato, T. Okazaki, H. Shinohara, S. Iijima. *Phys. Rev. Lett.,* **85**, 5384 (2000); K. Suenaga, M. Tence, C. Mory, C. Colliex, H. Kato, T. Okazaki, H. Shinohara, K. Hirahara, S. Bandow, S. Iijima. *Science,* **290**, 2280 (2000).
[3] B.W. Smith, D.E. Luzzi, Y. Achiba. *Chem. Phys. Lett.,* **331**, 137 (2000).
[4] A.N. Khlobystov, K. Porfyrakis, M. Kanai, D.A. Britz, A. Ardavan, H. Shinohara, T.J.S. Dennis, G.A.D. Briggs. *Angew. Chem. Int. Ed.,* **43**, 1386 (2004).
[5] K. Urita, Y. Sato, K. Suenaga, A. Gloter, A. Hashimoto, M. Ishida, T. Shimada, H. Shinohara, S. Iijima. *Nano Lett.,* **4**, 2451 (2004).
[6] F. Simon, H. Kuzmany, H. Rauf, T. Pichler, J. Bernardi, H. Peterlik, L. Korecz, F. Fülöp, A. Jánossy. *Chem. Phys. Lett.,* **383**, 362 (2004).
[7] B. Corzilius, A. Gembus, N. Weiden, K.-P. Dinse. In: *Electronic Properties of Novel Nanostructures*, H. Kuzmany, J. Fink, M. Mehring, S. Roth (Eds.), AIP Conference Proceedings **786**, pp. 317–320 (2005); B. Corzilius, A. Gembus, K.-P. Dinse, F. Simon, H. Kuzmany. In: *Electronic Properties of Novel Nanostructures,* H. Kuzmany, J. Fink, M. Mehring, S. Roth (Eds.), AIP Conference Proceedings **786**, pp. 291–295 (2005).
[8] J.C. Greer. *Chem. Phys. Lett.,* **326**, 567 (2000).
[9] B. Pietzak, A. Weidinger, K.-P. Dinse, A. Hirsch. In: *Group V Endohedral Fullerenes: N@C_{60}, N@C_{70}, and P@C_{60}*, T. Akasaka and S. Nagase (Eds.), Kluwer Academic Publishers, Dordrecht, pp. 13–66 (2002).
[10] B. Pietzak, M. Waiblinger, T. Almeida Murphy, A. Weidinger, M. Höhne, E. Dietel, A. Hirsch. *Chem. Phys. Lett.,* **279**, 259 (1997).
[11] P. Jakes, K.-P. Dinse, C. Meyer, W. Harneit, A. Weidinger. *Phys. Chem. Chem. Phys.,* **5**, 4080 (2003).
[12] B. Corzilius, K.-P. Dinse, K. Hata. *Phys. Chem. Chem. Phys.,* 2007, DOI: 10.1039/b707936m.
[13] K. Hata, D.N. Futaba, K. Mizuno, T. Namai, M. Yumura, S. Iijima. *Science,* **306**, 1362 (2004).
[14] M. Yudasaka, K. Ajima, K. Suenage, T. Ichihashi, A. Hashimoto, S. Iijima. *Chem. Phys. Lett.,* **380**, 42 (2003).
[15] N. Weiden, B. Goedde, H. Käß, K.-P. Dinse, M. Rohrer. *Phys. Rev. Lett.,* **85**, 1544 (2000).
[16] T.J.S. Dennis, K. Prassides, E. Roduner, L. Cristofolini, R. DeRenzi. *J. Phys. Chem.,* **97**, 8553 (1993).
[17] P. Jakes, N. Weiden, R.-A. Eichel, A. Gembus, K.-P. Dinse, C. Meyer, W. Harneit, A. Weidinger. *J. Magn. Res.,* **156**, 303 (2002).
[18] J.J.L. Morton, A.M. Tyryshkin, A. Ardavan, K. Porfyrakis, S.A. Lyon, G.A.D. Briggs. *J. Chem. Phys.,* **124**, 014508 (2006).
[19] B. Corzilius, K.-P. Dinse, K. Hata. *phys. stat. sol. (b),* **243**, 3273 (2006).
[20] A. Schweiger and G. Jeschke. *Principles of pulse electron paramagnetic resonance*, pp. 431–443, Oxford University Press, Oxford, UK (2001).
[21] A.V. Astashkin and A. Schweiger. *Chem. Phys. Lett.,* **174**, 595 (1990).